Energy Storage Bidirectional DC-DC Converter Model Predictive Control

Feng Zhao, Dong Li*, Xiaoqiang Chen, and Ying Wang

School of Automation and Electrical Engineering, Lanzhou Jiaotong University, Lanzhou 730070, China

Corresponding author. E-mail: 1697949784@qq.com

Aiming at the voltage fluctuation of DC microgrid bus caused by the power fluctuation of distributed power supply and switching of constant power load (CPL), this paper proposes a model predictive control (MPC) strategy with nonlinear observer, which is applied to bidirectional DC-DC converter for energy storage. First, a small disturbance model of the system with converter control is established, the influence of photovoltaic unit and constant power load on the system stability is analyzed, and then the objective function is constructed according to the bidirectional DC-DC converter, the optimization equation is established and the optimal control rate is obtained. Second, a nonlinear state observer is established and a composite control strategy is designed to adjust the charging and discharging process of the battery, realize the power balance between the source and load of the DC microgrid, and ensure the stability of the DC microgrid. Finally, a simulation model is built in Simulink and the results are analyzed, and the simulation results show that the proposed control strategy has good dynamics and robustness compared with the traditional double-closed-loop PI control when the constant power load is frequently switched and the photovoltaic power generation power fluctuates.

1. Introduction

With the development of new energy, DC microgrid has become an indispensable part of AC and DC hybrid distribution network [1]. With the abundance of DC microgrid application scenarios and the increasing number of DC equipment at the source and load ends, the stability of its system cannot be ignored for the safe operation of DC microgrid. Compared with AC microgrids, DC microgrids have the following outstanding advantages: distributed power sources and energy storage equipment are mostly in DC form, which makes it easier to access DC microgrids without considering the tracking of voltage and frequency; a large number of power electronic loads are supplied with DC power through the converter, which improves the conversion efficiency between systems and greatly improves reliability; the structure is simpler than the AC microgrid. In the DC microgrid, the most intuitive indicator that can

reflect the stability of the system is the DC bus voltage, in general, there are mainly the following three factors can affect the DC bus voltage: That is, the distributed power output power determined by natural conditions fluctuates, the load fluctuation of the load side is mainly based on constant power load, and the energy exchange between the AC large grid and the DC microgrid in the switching and grid-connected operation mode [2]. The protection device in the DC microgrid will trigger the protection action at the moment when the DC bus voltage is unstable. The DC bus voltage fluctuation will affect the power quality, and in severe cases, the whole power grid system will collapse. For such voltage fluctuations, photovoltaic fluctuations and load fluctuations are mostly smoothed out by power electronic converter control [3].

Since many power electronic conversion units with nonlinear characteristics are included in the DC microgrid sys-

tem, such as the closed-loop control power electronic converter, it can be regarded as a constant power load (CPL) with complex impedance characteristics, which reduces the system damping [4, 5]. Therefore, the whole system has strong nonlinearity and time-varying characteristics [6, 7], and the traditional linear design method is no longer applicable. In order to solve the above problems, nonlinear design methods are introduced in the design of power electronic converters, among which the mainstream methods include exact feedback linearization (EFL) control, backstepping control, sliding mode variable structure (SMVS) control and model predictive control (MPC). The controller design idea in the literature [8] is based on exact feedback linearization, which can be applied to energy storage devices and has good performance, but this method is not universal, only suitable for specific systems under specific conditions. In the literature [9], the design method of sliding mode control is used to design a sliding mode controller applied to bidirectional energy storage converter, which has the advantages of easy design, strong robustness, and good adjustment of DC bus voltage. However, while maintaining the stability of the system, there will be another big problem, that is, the problem accompanied by jitter, which cannot be widely promoted in actual engineering. Literature [10] designs an integral backstepping controller for hybrid energy storage systems to ensure the power balance between source and load under variable power generation. However, the above design process has the problems of cumbersome design process and difficult parameter tuning.

Aiming at the problem of maintaining the stability of DC link voltage by energy storage bidirectional converter with CPL, this paper proposes a model predictive control (MPC) strategy with nonlinear state observer to switch the charge and discharge mode of energy storage device to solve the problem of power imbalance between source and load of isolated island DC microgrid. The proposed control strategy has a good control effect when the output of the photovoltaic unit decreases, faults and constant power load fluctuates.

2. Modeling analysis of small disturbances in the system with converter control

The DC microgrid studied in this paper is shown in Fig. 1. It consists of a photovoltaic power generation unit, an energy storage device and a CPL load. Among them, the energy storage converter adopts the bidirectional Boost-Buck topology, U_b is the battery voltage, L_b, i_{Lb}, i_{Lb1} are the energy storage converter inductor, the current flowing through the inductor and the converter output current, d_1 is the switch S_1 modulation signal, S_1 and S_2 use com-

plementary modulation, and U_{dc} is the bus voltage. The photovoltaic unit adopts the Boost topology, U_a is the photovoltaic voltage, $L_a, i_{La},$ and i_{La1} are the inductor, inductor current and converter output current of the Boost converter, respectively, and d_2 is the S_3 modulation signal. The load converter adopts the Buck topology, L_1 and i_{L1} are the Buck converter inductor and inductor current, d_3 is the switch S_4 modulation signal, and i_1 is the input current of the Buck converter.
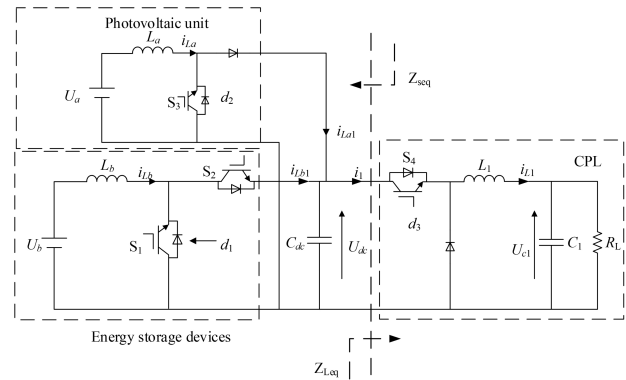
Fig. 1. DC microgrid topology

The photovoltaic converter adopts MPPT control, the energy storage converter and the load converter are controlled by constant voltage PI, and Fig. 2 is the control block diagram of the three converters.

(a)

(b)

(c)
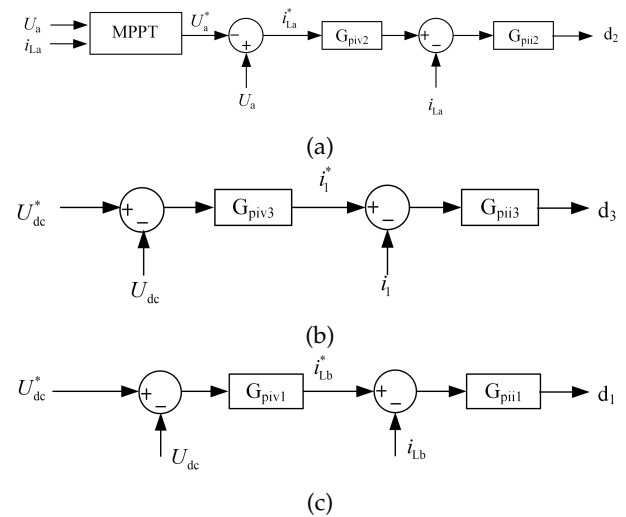
Fig. 2. Transformer control block diagram

Among them, G_{piv1} and G_{pii1} are the transfer functions of the voltage and current loop PI links of the energy storage converter, $G_{piv1} = K_{pv1} + K_{iv1}/s, G_{pii1} = K_{pi1} + K_{ii1}/s, K_{pv1}$ and K_{iv1} are the voltage loop proportions and integration coefficients, and K_{pi1} and K_{ii1} are

the current loop proportions and integration coefficients. G_{piv2}, G_{pii2} and G_{piv3}, G_{pii} have the same meanings as above. The small disturbance model of the energy storage system of the fixed voltage control energy storage system can be obtained by linearizing the topology of the energy storage converter and the operating point of the differential equation.

$$\frac{d\Delta u_{dc}}{dt} = \frac{1}{C_{dc}} \left[(1 - D_1) \Delta i_{Lb} - I_{Lb}\Delta d_1 - \Delta i_{Lb1} \right]$$

$$\frac{d\Delta i_{Lb}}{dt} = \frac{-1}{L_b} \left[(1 - D_1) \Delta u_{dc} - U_{dc}\Delta d_1 \right]$$

$$\frac{d\Delta i_{Lb}^*}{dt} = -K_{pv1}\frac{d\Delta u_{dc}}{dt} - K_{iv1}\Delta u_{dc}$$

$$\frac{d\Delta d_1}{dt} = K_{pi1} \left(\frac{d\Delta i_{Lb}^*}{dt} - \frac{d\Delta i_{Lb}}{dt} \right) + K_{ii1} \left(\Delta i_{Lb}^* - \Delta i_{Lb} \right) \tag{1}$$

The input impedance of the energy storage converter is obtained by solving the above Lasse transform

$$Z_{sin} = \frac{\Delta u_{dc}}{-\Delta i_{Lb1}} = \frac{B_s}{A_s}$$

$$A_s = sC_{dc} - I_{Lb}G_{pii1}G_{piv1}$$

$$- \frac{\left(1 - D_1 + I_{Lb}G_{pii}\right)\left(D_1 - 1 - U_{dc}G_{pii1}G_{piv1}\right)}{\left(sL_b + U_{dc}G_{pii1}\right)} \tag{2}$$

$$B_s = 1$$

The same applies to the input impedance of the photovoltaic converter

$$Z_{pvin} = \frac{\Delta u_{dc}}{-\Delta i_{La1}} = \frac{1}{A_{pv}}$$

$$A_{pv} = sC_{dc} + \frac{\left(1 - D_2 + I_{La}G_{pii2}\right)\left(1 - D_2\right)}{\left(sL_a - U_a/I_{La} + U_{dc}G_{pii2}\right)} \tag{3}$$

Load converter input impedance

$$Z_{Llin} = \frac{\Delta u_{dc}}{\Delta i_1} = \frac{B_{L1}}{A_{L1}}$$

$$B_{L1} = sL_1 + U_{dc}G_{pii3} + \frac{\left(1 + U_{dc}G_{pi3}G_{piv3}\right)}{sC_1 + G_{L1}}$$

$$A_{L1} = D_3^2 - G_{pii3}D_3I_{L1}\left(\frac{G_{piv3}}{sC_1 + G_{L1}} + 1\right) \tag{4}$$

$$G_{L1} = 1/R_L$$

Among them, D_1, D_2 and D_3 are the steady-state components of the duty cycle of the energy storage, photovoltaics and load converters, respectively.

If the equivalent output impedance at the source side is Z_{seq} and the equivalent input impedance at the load side is Z_{leq}, the loop gain T_m is:

$$T_m = \frac{Z_{sin}Z_{pvin}}{Z_{Lin}\left(Z_{sin} + Z_{pvin}\right)} \tag{5}$$

Among them, Z_{sin}, Z_{pvin}, and Z_{Lin} have small disturbance input impedances for energy storage, photovoltaics, and load converters, respectively.

According to the dominant pole change trajectory of the port closed-loop transfer function $(1 + T_m)^{-1}$, the influence of photovoltaic power supply and constant power load change on the system stability is analyzed:

Fig. 3 shows the trajectory diagram of the dominant pole with CPL when there is photovoltaic input, so that the power of CPL accumulates from 500 W, and with the gradual increase of P_{cpl}, a pair of conjugated dominant poles of its closed-loop transfer function moves to the right and crosses the virtual axis around 3000 W in P_{cpl}, and the system is unstable. Fig. 4 is the trajectory of the dominant pole with CPL when there is no photovoltaic input, compared with Fig. 3, with the increase of P_{cpl}, the dominant pole moves to the right but does not cross the imaginary axis, and the system remains stable, which proves that the photovoltaic input reduces the system stability. Fig. 5 shows the change trajectory of the dominant pole with the photovoltaic power P_{pv} when there is photovoltaic input, and compared with Fig. 3, it can be obtained that the change of photovoltaic power has little impact on the system stability.
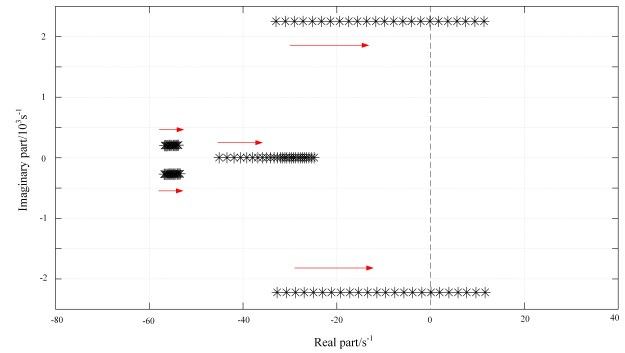
Fig. 3. When PV is put in, the dominant pole changes the trajectory with CPL

In summary, the increase of CPL power, the input of photovoltaic cells and the increase of photovoltaic unit output will reduce the system stability, but the first two have a greater impact, so this paper mainly studies the impact of photovoltaic power change and CPL power change on the system stability during photovoltaic input.

3. Energy storage converter modeling

The photovoltaic power generation unit of the microgrid system shown in Figure 1 works in the MPPT control mode,
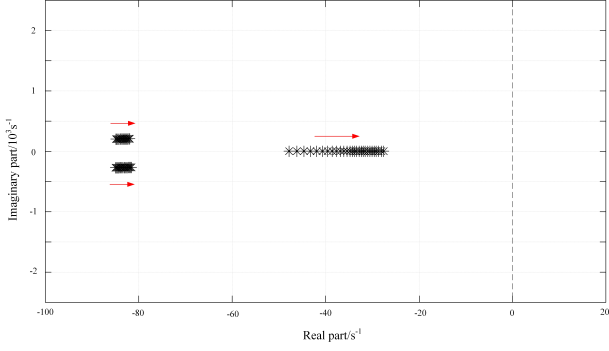
Fig. 4. Without PV input, the dominant pole changes the trajectory with CPL
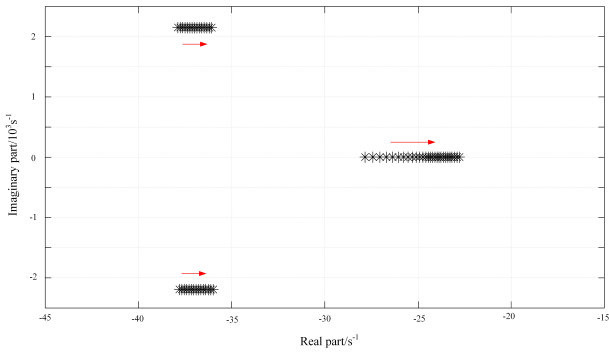
Fig. 5. When PV is put in, the dominant pole changes with P_{pv}

and the bus voltage stability of the DC microgrid mainly depends on the regulation of the energy storage unit, and the energy storage unit can adjust its charge and discharge mode according to the power of the load end of the source end, thereby maintaining the stability of the power grid. The load is connected to the bus bar through a closed-loop control converter, which is regarded as a constant power load CPL, which has negative impedance characteristics to the outside and is modeled as $i_{CPL} = P_{cpl}/U_{dc}$.

For this microgrid structure, it can be simplified as shown in Fig. 6.

Through the state averaging method, the dynamic equation of the bidirectional DC/DC converter at the energy storage end is obtained according to Fig. 6:

$$\begin{cases} \frac{di_{Lb}}{dt} = \frac{1}{L_b}(d_1 - 1)U_{dc} + \frac{U_b}{L_b} \\ \frac{dU_{dc}}{dt} = \frac{1}{C_{dc}}i_{Lb}(d_1 - 1) + \frac{i_{La}}{C_{dc}} - \frac{P_{cpl}}{C_{dc}U_{dc}} \end{cases} \quad (6)$$

Formula: P_{cpl} is the constant power load power. There is an obvious nonlinear term P_{cpl}/U_{dc} in Eq. (6), which can be further expressed as follows:

$$\begin{cases} \frac{di_{Lb}}{dt} = A_i i_{Lb} + B_i u_i + F_i w_i \\ \frac{dU_{dc}}{dt} = A_v U_{dc} + B_v u_v + F_v w_v \end{cases} \quad (7)$$
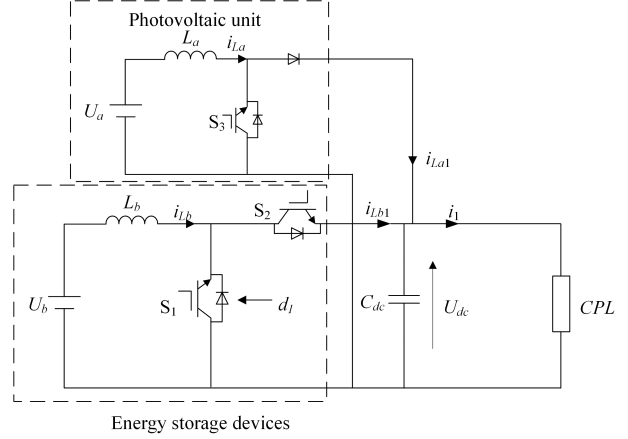
Fig. 6. Simplified model diagram of DC microgrid

Thereinto:

$$A_i = 0, \quad B_i = \frac{U_{dc}}{L_b}, \quad u_i = d_1 - 1,$$

$$F_i = \frac{1}{L_b}, \quad w_i = U_b + \beta_i$$

$$A_v = 0, \quad B_v = \frac{i_{Lb}}{C_{dc}}, \quad u_v = d_1 - 1,$$

$$F_v = \frac{1}{C_{dc}}, \quad w_v = i_{La} - \frac{P_{cpl}}{U_{dc}} + \beta_v$$

where , β_i, β_v represents the model uncertainty. To simplify the design, assume that:

$$\lim_{t \to \infty} \beta_i = 0, \quad \lim_{t \to \infty} \beta_v = 0$$

4. Mpc controller design

4.1. Model prediction

For a single input single output system there is

$$y = Ay + Bu + Fw \quad (8)$$

Where: y is the state of the system, u is the control input, w is the sum of multiple perturbations composed of the uncertainty of the model and the external perturbations. Define the objective function of the system represented by the above equation as

$$J = [e(t + T_r)]^2 = [y_{ref}(t + T_r) - y(t + T_r)]^2 \quad (9)$$

Where: T_r is the prediction time, $y_{ref}(t + T_r)$ is the output reference value. Expanding the Taylor series to the above equation, there are:

$$e(t + T_r) = e(t) + T_r e^{(1)}(t) + \ldots + \frac{T_r^{\sigma+r}}{(\sigma + r)!}e^{(\sigma+r)}(t) \quad (10)$$

where: σ is the relative degree of the system, r is the control order; In this paper, the relative degree is 1 and the control order is 0 , so eliminate the higher-order derivatives and simplify the above equation to:

$$e\left(t + T_{\mathrm{r}}\right) = e(t) + T_{\mathrm{r}}e^{(1)}(t) \tag{11}$$

It can be obtained using Eq. (8) and Eq. (9).

$$\dot{e}(t) = \dot{y}_{\mathrm{ref}}(t) - \dot{y} = \dot{y}_{\mathrm{ref}}(t) - Ay - Bu - Fw \tag{12}$$

Eq. (11) is further expressed as:

$$\left(t + T_{\mathrm{r}}\right) = e(t) + T_{\mathrm{r}}\left(\dot{y}_{\mathrm{ref}} - Ay - Bu - Fw\right) \tag{13}$$

Bringing the above equation into the objective function of Eq. (9) yields:

$$J = \left(\boldsymbol{H}(y) - \boldsymbol{G}u - \boldsymbol{M}w\right)^{T}\boldsymbol{Y}\left(T_{r}\right)\left(\boldsymbol{H}(y) - \boldsymbol{G}u - \boldsymbol{M}w\right) \tag{14}$$

Where: $\boldsymbol{H}(y) = \begin{bmatrix} e(t) & \dot{y}_{\mathrm{ref}}(t) - Ay \end{bmatrix}^{T}$, $\boldsymbol{G} = \begin{bmatrix} 0 & B \end{bmatrix}$, $\boldsymbol{M} = \begin{bmatrix} 0 & F \end{bmatrix}$.

Let the objective function control the derivative of the input $\frac{dJ}{du} = 0$ to obtain the optimal control rate:

$$u(t) = \frac{1}{B}\left(\frac{1}{T_{\mathrm{r}}}e(t) + \dot{y}_{\mathrm{ref}} - Ay - Fw\right) \tag{15}$$

Substituting Eq. (15) into Eq. (12) yields an error equation representing a

closed-loop system

$$\dot{e}(t) + \frac{1}{T_{\mathrm{r}}}e(t) = 0 \tag{16}$$

Since the prediction time is always positive, the system is progressively stable. Since in practice, perturbations are not always measured in real time, Eq. (15) can be rewritten as:

$$u(t) = \frac{1}{B}\left(\frac{1}{T_{\mathrm{r}}}e(t) + \dot{y}_{\mathrm{ref}} - Ay - F\hat{w}\right) \tag{17}$$

where: $\hat{w}$ is an estimate of w.

4.2. Perturbation observer design

When using MPC to control the converter, the robustness and control effect of the system will be affected due to the inaccuracy of the model and external interference. Therefore, a nonlinear disturbance observer is designed to solve the above problems.

$$\begin{cases} \hat{w} = \lambda(y - z) \\ \dot{z} = Ay + Bu + F\hat{w} \end{cases} \tag{18}$$

where z is the estimated value of the output y, λ is the observer gain, and the derivative of the perturbation estimate can be expressed as

$$\dot{\hat{w}} = \lambda(\dot{y} - Ay - Bu - F\hat{w}) \tag{19}$$

Defining the estimation error $e_{w} = \hat{w} - w$, combine Eq. (8) with Eq. (19) to

obtain the dynamic equation for the observer

$$\dot{e}_{w} + \lambda F e_{w} = -\dot{w} \tag{20}$$

It is clear that a suitable observer can be selected to gain λ such that $\lambda F > 0$. Thus the bounded error of the estimation depends on w, assuming $\lim_{t\to\infty} w = 0$, when $t \to \infty$ the observer is clearly asymptotically stable.

Substituting Eq. (17) into Eq. (18) gives the derivative of the system perturbation estimate

$$\dot{\hat{w}} = -\frac{\lambda}{T_{\mathrm{r}}}e(t) - \lambda\dot{e}(t) \tag{21}$$

The simplified perturbation estimate can be obtained from the integral of the above equation:

$$\hat{w}(t) = -\frac{\lambda}{T_{\mathrm{r}}}\int_{0}^{t}e(\tau)d\tau - \lambda e(t) + \lambda e(0) + \hat{w}(0) \tag{22}$$

4.3. Integrated control approach

In practice, the perturbation can be seen as the sum of the measurable perturbation W_{m} and the unknown perturbation W_{u}, so Eq. (17) can be written as:

$$u(t) = \frac{1}{B}\left(\frac{1}{T_{\mathrm{r}}}e(t) + \dot{y}_{\mathrm{ref}} - Ay - Fw_{\mathrm{m}} - F\hat{w}_{\mathrm{u}}\right) \tag{23}$$

The unknown perturbation estimate can be obtained from Eq. (22).

Let $\lambda e(0) + \hat{w}(0) = 0$, substituting Eq. (22) into Eq. (23) yields the final expression of the law of control as follows:

$$u(t) = \frac{1}{B}\left(\left(\frac{1}{T_{\mathrm{r}}} + \lambda F\right)e(t) + \frac{\lambda F}{T_{\mathrm{r}}}\int_{0}^{t}e(\tau)d\tau + \left(\dot{y}_{\mathrm{ref}} - Ay - Fw_{\mathrm{m}}\right)\right) \tag{24}$$

The model predicted control designed in this paper adopts voltage and current double-loop control, and the inner loop control law can be obtained by combining Eq. (7) and Eq. (24):

$$u_{i}(t) = \frac{1}{U_{\mathrm{dc}}}\left(\left(\frac{L_{\mathrm{b}}}{T_{\mathrm{ri}}} + \lambda_{i}\right)e_{i}(t) + \frac{\lambda}{T_{\mathrm{r}}}\int_{0}^{t}e_{i}(\tau)d\tau - U_{\mathrm{b}}\right) \tag{25}$$

Outer loop control law:

$$u_{v}(t) = -\frac{1}{i_{\mathrm{Lb}}}\left(\left(\frac{C_{\mathrm{dc}}}{T_{\mathrm{rv}}} + \lambda_{v}\right)e_{v}(t) - \frac{\lambda}{T_{\mathrm{r}}}\int_{0}^{t}e_{v}(\tau)d\tau + i_{\mathrm{La}}\right) \tag{26}$$

In summary, the control block diagram of the proposed method is shown in Fig. 7.
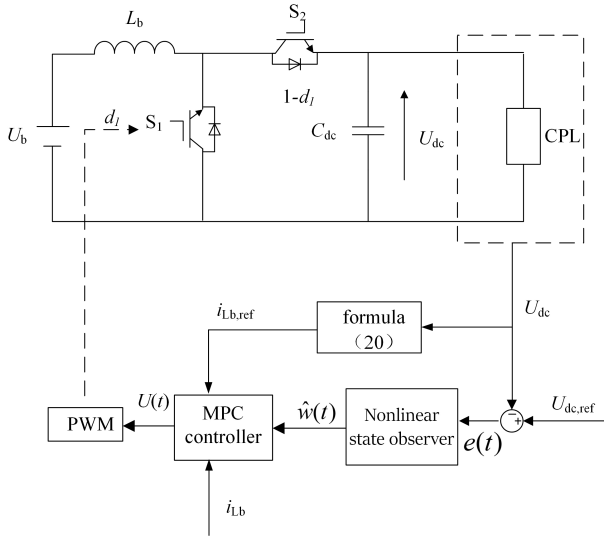
Fig. 7. The control block diagram mentioned in this article

5. Analysis of simulation results

The parameters of the DC microgrid system shown in Fig. 6 are shown in Table 1, and a complete simulation model is built on the Simulink simulation platform for verification. In order to study the problem of maintaining the stability of the DC link voltage of the energy storage bidirectional converter with CPL and the effectiveness of the proposed control strategy, a verification analysis is performed in this section under three different working conditions.

Assuming that under the condition of sufficient light, the demand power of the load end is less than the output power of the photovoltaic unit, the overflow power of the photovoltaic unit will be stored in the battery energy storage unit, and the energy storage unit at this time is in the step-down charging working mode. In order to verify the controller's ability to adjust the energy storage unit to maintain system stability, this paper simulates under the following two common working conditions, namely, the decrease in light intensity of working condition 1 leads to a change in PV output and the failure of the PV unit in working condition 2 leads to no output of the PV cell. The control effect of the model designed in this paper on the DC link voltage of the predictive controller and the traditional PI dual-closed-loop controller is compared.

Working condition 1: The light intensity decreases. In the simulation system, the light intensity of the photovoltaic power generation module is continuously reduced from the original 1000 W/m² to 800 W/m². At this time,

the output power of the photovoltaic unit drops to the demand power of the load side, and the battery ends the charging mode, as shown in Fig. 8, the change of photovoltaic power and battery power when the light intensity changes:
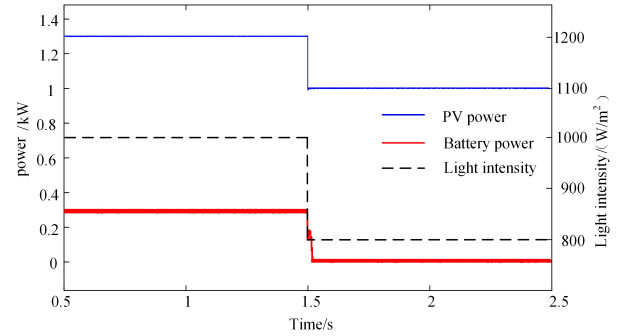
Fig. 8. The power of each unit changes when the light intensity changes

As shown in the adjustment process shown in Fig. 9, within $0 \sim 1.5$ s, the SOC continues to increase to 60.0019%, and at 1.5 s, the battery current changes from -5 A to 0 A, and the SOC first increases and then remains unchanged. As shown in Fig. 10, there will be voltage fluctuations during the battery regulation process, which is due to the instantaneous power imbalance between the source end and the load end of the DC microgrid during the switching of the state of the energy storage unit, resulting in voltage fluctuations.
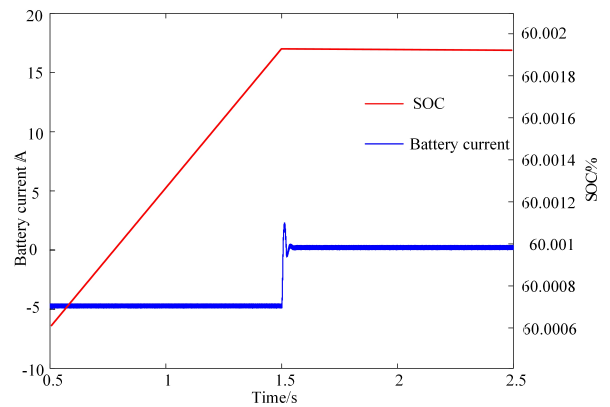
Fig. 9. The state of the battery changes when the light intensity changes

Under the regulation of the MPC controller designed in this paper, the DC link voltage fluctuates between $105 \sim 112$ V, the maximum voltage deviation is 4.5%, and the 110 V remains stable after 0.04 s, compared with the double closed-loop PI control effect is not as good as the control

Table 1. DC microgrid system parameters

Parameter	DC link capacitance / /mF	Voltage reference value $V_{rer/V}$	Line inductance /mH	Forecast period T/s	Switching frequency fkHz
Pumeric value	1.4	110	5	0.002	20
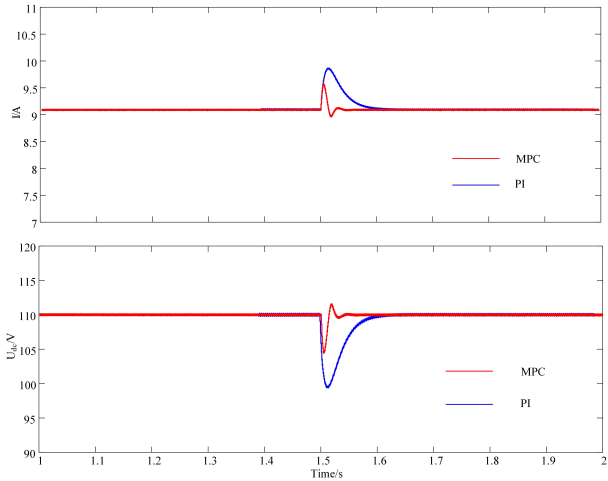
Fig. 10. Busbar voltage and current regulation process when illumination changes

strategy mentioned in this paper in terms of response speed and suppression of bus voltage fluctuation.

Working condition 2: PV fault shutdown. When t = 4 s, the photovoltaic power generation unit is completely cut off in the simulation system. At this time, due to the demand power at the load end, the battery switches to the boost discharge working mode through the bidirectional energy storage converter, as shown in Fig. 11 is the change of photovoltaic voltage and battery power when the photovoltaic unit fails.
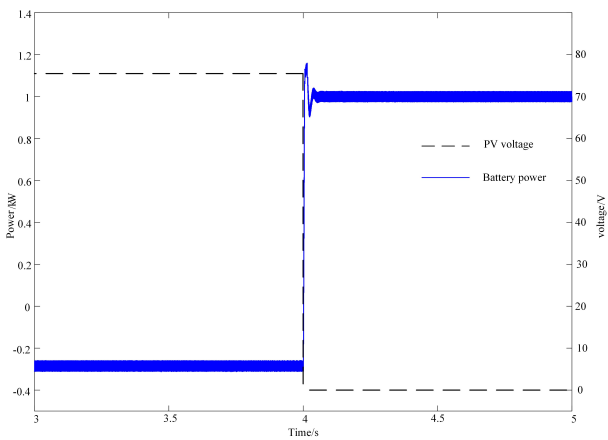
Fig. 11. Power change of each unit during PV failure

In the process of charging and discharging the battery shown in Fig. 12, within $0 \sim 4$ s, due to sufficient light, the output power is greater than the demand power, and the energy storage unit works in the charging mode. At 4 s, the photovoltaic unit fails, and the energy storage unit ends charging and enters the step-up discharge working mode. Fig. 13 shows the regulation process of bus voltage and current during photovoltaic failure, it can be seen that under the regulation of the MPC controller designed in this paper, the DC bus voltage fluctuates at $100 \sim 113$ V, the maximum voltage deviation is 9%, and it remains stable after 0.05 s recovery to 110 V. With PI controller, the fluctuation amplitude and adjustment time of the bus voltage are much larger than the controller mentioned in this article.
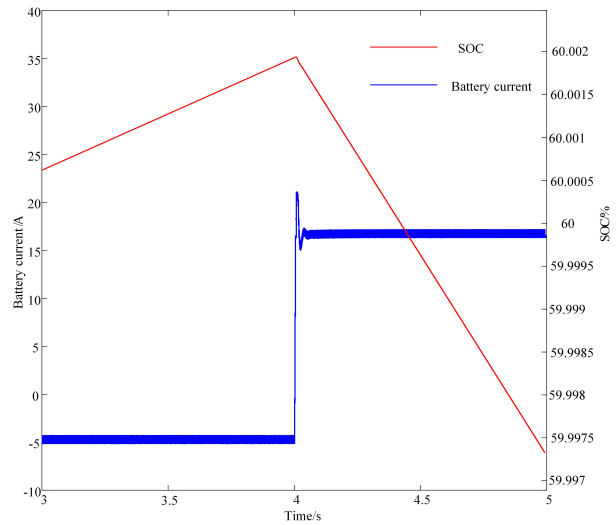
Fig. 12. Battery state change during PV failure

Working condition 3: Load sudden changes lead to bus voltage fluctuations. Unlike the positive impedance characteristics of resistive loads, constant power loads have negative impedance characteristics, and it is precisely because of their negative impedance characteristics that the damping of the system is reduced and the system is more prone to instability. In this paper, only the worst-case scenario, that is, only the constant power load is connected to the DC bus, and on this basis, the stability of the proposed controller is verified. In order to simulate the sudden change of load,
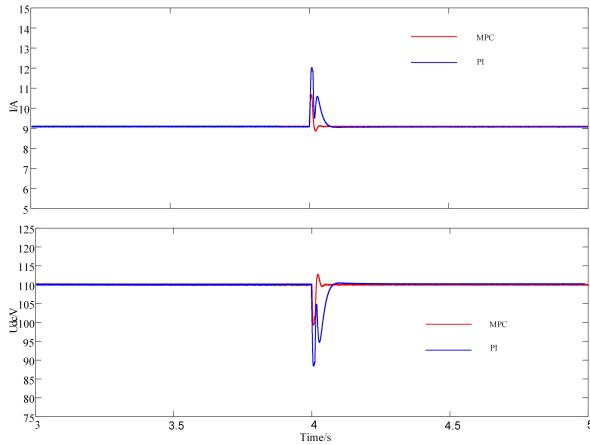
Fig. 13. Busbar voltage and current regulation during PV fault

the constant power load is changed from 800 W to 1000 W at t = 5 s, from 1000 W to 1500 W at t = 5.5 s, and from 1500 W to 3000 W at $t = 6$ s.

As shown in Fig. 14, at t = 5 s and t = 5.5 s, the CPL increases to 1500 W, and the proposed controller and the traditional PI controller can keep the system stable, and at t = 6 s the CPL continues to increase to 3000 W, and the system under the PI controller becomes unstable, which is consistent with the analysis results in Fig. 3, and the controller proposed in this paper can keep the system stable, which verifies the advantages of the proposed controller in maintaining the system stability.
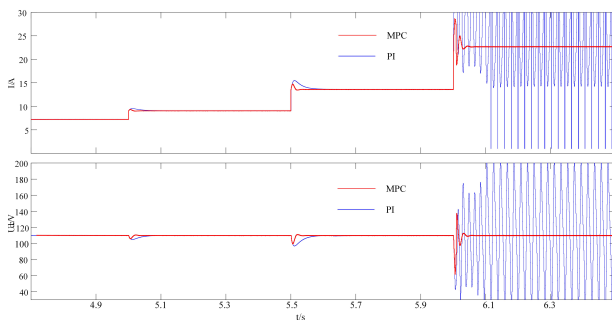
Fig. 14. Bus voltage and current regulation during sudden load changes

In order to compare the control strategy proposed in this paper with the model prediction controller without observers, the load is changed from 500 W to 1000 W at t = 7.5 s and back to 500 W at t = 8.5 s. As can be seen from Fig. 15, the MPC controller without the observer cannot accurately track the voltage reference value when the load changes abruptly, and the deviation from the voltage

reference value is 2 V. The controller mentioned in this article can track the bus voltage well and keep the DC bus voltage stable, which indicates that the controller has the advantage of tracking the voltage without deviation.
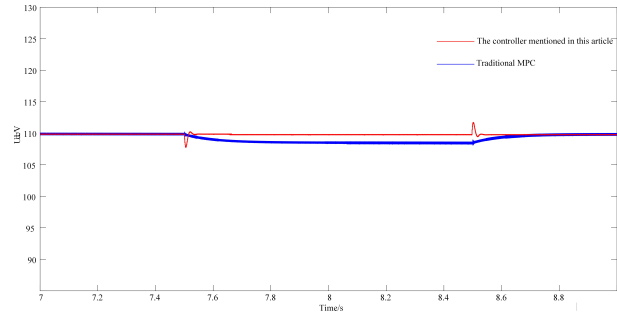
Fig. 15. Comparison of the proposed MPC and traditional MPC

In summary, under the action of the control strategy proposed in this paper, the DC link voltage response speed is faster, the fluctuation is small, and the control effect is higher.

6. Conclusions

Aiming at the problem of maintaining the stability of DC bus voltage in energy storage bidirectional DC-DC converter with CPL, this paper designs an MPC controller applied to energy storage bidirectional converter, which has a simple design process and can play a good role in the stability of DC bus voltage, and has the following conclusions.

1. In terms of feasibility, in view of unknown disturbances and load changes in the system, the MPC with state observer mentioned in this paper has the advantages of simple design process and easy implementation compared with the backstepping controller and sliding mode controller.

2. In terms of robustness, the MPC control strategy with condition observer has the function of accurately tracking and adjusting the bus voltage without bias. It is very robust to external interference and uncertainty of the system.

3. In terms of control performance, compared with traditional PI control and MPC control, the control strategy proposed in this paper is superior to the former in improving the transient performance of bus voltage and accurate tracking without bias, and has higher control performance.

References

[1] L. Zekun, K. Li, P. Wei, Yehua, and D. Wei, (2018) *"Stability analysis of large disturbances in sag-controlled DC microgrids based on hybrid potential function"* **Grid Technology** *42*(11): 10.

[2] W. Chengshan, L. Wei, W. Xifeng, M. Zhun, and Y. Liang, (2017) *"A Review of DC Microgrid Bus Voltage Fluctuation Classification and Suppression Methods"* **Chinese Journal of Electrical Engineering** *37*(1): 84–97.

[3] F. Jianjun, (2021) *"The role and application of energy storage in photovoltaic low-voltage DC-powered buildings"* **Energy Storage Science and Technology** *10*(2): 624.

[4] M. Jianhui, Z. Peigen, W. Yi, and W. Chen, (2019) *"Small-signal modeling and parametric analysis of DC microgrid based on flexible virtual inertial control"* **Journal of Electrical Engineering Technology** *34*(12): 2615–2626.

[5] M. Cespedes, L. Xing, and J. Sun, (2011) *"Constant-power load system stabilization by passive damping"* **IEEE Transactions on Power Electronics** *26*(7): 1832–1836.

[6] M. Zhao, Z. Zhigang, S. Yuanyuan, L. Yahui, and L. Kejun, (2019) *"Key Technologies and Development Prospects of New Generation Low Voltage DC Power Supply System"* **Power System Automation** *43*(23): 12–22.

[7] Z. Baoge, Z. Zhen, W. Donghao, L. Ping, and Ronyao, (2020) *"A Bidirectional DC/DC Converter for Composite Energy Storage"* **Energy Storage Science and Technology** *9*(1): 178.

[8] X. Shao, J. Hu, and Z. Zhao, (2019) *"Stabilisation strategy based on feedback linearisation for DC microgrid with multi-converter"* **The Journal of Engineering** *2019*(16): 1802–1806.

[9] B. Ye, Y. Liu, and Z. Wu. "Research on Sliding Mode Control Strategy for Bidirectional DC/DC Energy Storage Converter". In: *2019 IEEE International Conference on Electron Devices and Solid-State Circuits (EDSSC)*. IEEE. 2019, 1–3.

[10] H. Armghan, M. Yang, M. Wang, N. Ali, and A. Armghan, (2020) *"Nonlinear integral backstepping based control of a DC microgrid with renewable generation and energy storage systems"* **International Journal of Electrical Power & Energy Systems** *117*: 105613.